ISSN: 2141 – 3290
www.wojast.com

OPTIMIZING SOLAR TRACKER DEVICE USING PROPORTIONAL INTEGRAL CONTROLLER

[1]ODUOBUK, E. J., [2]OBIANWU, V. I. AND [3]AKPABIO, I. O.
[1&3]*Department of Physics, University of Uyo*
[2]*Department of Physics, University of Calabar*
enobong_joseph1@yahoo.com

ABSTRACT

Optimization of a solar tracker using proportion and integral controller was carried out to regulate the tracking process so that optimum energy is derived from the PV cell throughout the day time. The solar tracker control system was modeled and designed using MATLAB software. A mathematical approach was used to develop and model the sub-systems and the overall cascade system transfer function equations, which include the inner and outer PI controller loop transfer function, dynamic model of dc motor armature - controlled transfer function and photovoltaic cell domain equation transfer function. The simulink models of open and closed loop transfer functions of the sub-system and main process systems were also developed, simulated and analyzed, from where the performance and stability indices of the system are derived. Results of simulation yielded a relatively low in rise time, settling time and steady state error of 0.4s, 1.8s and 0.0 rad/s. The results also showed that coupling proportional integral controller with photovoltaic cell reduces rise and settling time to a relatively low value of 1.6s and 5.5s respectively. Hence, using a proportional integral controller on solar tracking has reduced the rise time performance index by 77.8% and caused system stability to decrease to 67.2%, as compared to the existing system. The results imply that with proportional integral controller, it takes a shorter time for the solar tracker to respond to sudden change in input signal and quickly positions the photovoltaic cell at desired angle. The shorter time and speed achieved in this system means that only smaller amount of power would be required to position the PV cell appropriately. Therefore, PI controller is highly recommended for solar energy tracking because it is capable of reducing the system rise time, settling time and eliminate overshoot, undershoot, steady state error.

INTRODUCTION

Most solar panels generate low output due to the sun's movement in the day time. This unstable source of solar radiation due to rotation of the Earth has resulted in most solar panel systems becoming under-utilized and recording relatively low output efficiency. Also, the output voltage of the PV module reduces as module temperature increases, and most solar tracker designs are voltage based when the PV cell output current is unaffected by increase in temperature.

Moreover, when mounting PV modules on the roof, the PV module heat up substantially as inner temperatures increases from 50 – 75 ^{0}C. It means that a huge percentage of the power tracked or harvested from the sun is almost used up during the tracking process. This paper focuses on formulating appropriate models and methods of fully harnessing maximally the energy from the sun. The solution involves designing and developing models, including dynamic system of solar tracker using Proportional and Integral (PI) controllers, to control and position solar panel (PV cell), enhance cooling and optimize the solar tracking capabilities in terms of speed and accuracy.

Solar energy is gradually gaining global attention due to the growing need of clean and sustainable power supply, many have carried out researches using different methods and approaches which yield some results but also create research gaps. For instant Bamigboye *et al.* (2016), developed a solar tracking system using Internal Model Control (IMC-PID) controller. PID controller was used coupled with Internal Model Control (IMC). The research showed that

the systems slowest rise and settling time, the presence of sensor and D controller component makes the system complex and bulky.

Kiyak and Gokhan (2016), did a comparison of fuzzy logic and PID controller for a single-axis solar tracking system. Result showed that the system had only one dimension of rotation, voltage based tracker and complex. Kumar and Sharma (2016), researched on improving performance of PV system using PID controller, but the approach lacked system operation analysis (rise and settling time), it is a one dimensional system, voltage based tracker and appear to be complex in practice. Kalanithi and Rajesh (2014), developed an MPPT controller based solar tracking system. The system used a method which leads to bulky system and voltage based tracker. Baranwal and Dwivedi (2014), developed a solar tracking system that has a fixed solar panel which maintains constant maximum power output. The work lacks frequency and time analysis, it is complex and bulky system. Ozerdem and Shahin (2014), developed a PV solar tracking system controlled by arduino/matlab/simulink. The system is a voltage based tracker system, it lacks operational concept (frequency and time analysis) and it is complex in practice. Balabel *et al.* (2013), worked on the design and performance of solar tracking photo-voltaic system. In the work, it employed voltage sensor which make the system complex with low accuracy and performance. Our work attempts to close the existing gaps highlighted above.

METHODOLOGY

The methodology employed in this research work involves control system design, development of control system model and control analysis. More details in modeling of system equations for inner and outer loop system controllers; proportional and integral (PI) controller loop transfer function, modeling of dc motor, dynamic model of armature controlled dc motor transfer function for would be analyzed. The mathematical modeling in electrical and mechanical domain, solar panel (photovoltaic cell); photovoltaic cell (solar panel) is also analyzed and expressed in terms of their transfer functions. Various system and subsystem SIMULINK are modeled in terms of open loop and closed loop transfer function. Also, the main process systems unit is developed and simulated using MATLAB software.

(a) System Modeling and Analysis

All the system's component used in this work were modeled and analyzed. They include system design, mathematical models, transfer function of sub-systems, and Simulink models. However, let's consider system design by decoupling and analyzing (Figure 1a).

(i) Proportional Integral (PI) Controller Loop Transfer function

From Figure 1a, we have that: $U\ (t)\ = K_p e_\theta(t) + K_i \int_0^t e_\theta\ (t)\ dt$

Taking Laplace transform of equation 1 L $[U\ (t)\ ]$ = L $[K_p e_\theta(t) + K_i \int_0^t e_\theta(t)\ dt]$

U (s) = $K_p E_\theta(s) + K_I \frac{1}{S} E_\theta(s)$

$$\boldsymbol{T.F_{PI}} = \frac{\boldsymbol{U(s)}}{\boldsymbol{E_\theta(s)}} = \frac{\boldsymbol{K_p S + K_I}}{\boldsymbol{S}} \qquad 1$$

(ii) Transfer Function of Dynamic Model of Armature Controlled DC Motor

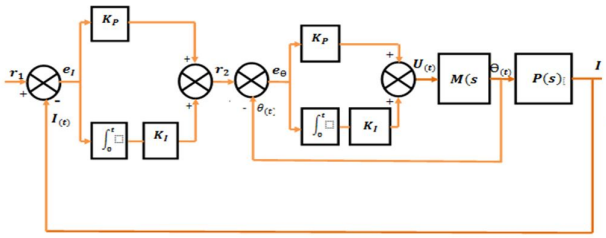

Fig.1a. Cascade control system block diagram of solar tracker

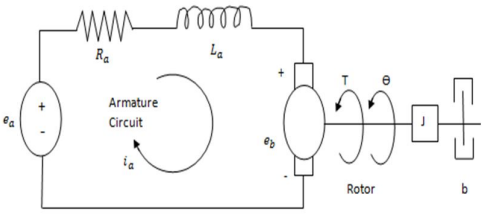

Fig. 1b. Equivalent circuit diagram of DC motor

Model Parameters and Assumptions

Let b = Friction or damping coefficient of the mechanical part of the rotor.

J = Rotational inertia of the rotor.

K = Motor torque or position of the coils with respect to the magnetic field (Constant)

$\vec{B}$ = Magnetic field constant

e_b = Back e.m.f induced in opposite direction, due to the moving coil in the magnetic field.

K_b = Back e.m.f Constant T = Torque produced by the motor rotor

From Lorentz's law we have; $\vec{F} = \overrightarrow{i_a} \times \vec{B}$ 2

$\overrightarrow{T} = K_1 B i_a$ 3

Where K_1 is a constant signifying the position of the coil relative to the magnetic field.

But since it is armature control, it means the K and B are constant. Therefore, equation 3 becomes

$T = Ki_a$ 4

From Faraday's Law, the back e.m.f induced in opposite direction is given as;

$e_b = K_b \frac{d\theta}{dt}$ 5

Where K_b = Back e.m.f constant.

(a) Electrical Domain Equation

Applying Kirchhoff Voltage Law (KVL) to the modeled circuit in (figure 1a) we have

$e_a - R_a i_a - L_a \frac{di}{dt} - e_b = 0$ 6

(b) Mechanical Domain Equation

Applying Euler's law (Sparavigna, 2015) the equation becomes $T - b\dot{\theta} = J\ddot{\theta}$ 7

Where $\dot{\theta}$ is speed of the motor, $\ddot{\theta}$ is the Angular Acceleration (rad/sec)

$T - b\dot{\theta}$ is the sum of the Moment.

In this case, before the electrical domain is coupled to mechanical domain, we first realize that the back e.m.f depends on the speed of the rotor while the torque is a function of the electric current, then we classified our output as position in terms of angle ($\theta_{(s)}$) and $E_{(s)}$ as input component.

However, since the Transfer Function (TF) of the dc motor is expressed;

$T.F = \frac{Position}{Volatge} = \frac{\Theta(s)}{E_a(s)}$ 8

Substituting equation 5 into 6 we have equation for electrical domain to be;

$e_a - R_a i_a - L_a \frac{di}{dt} - K_b\dot{\theta} = 0$ 9

In this case equation 9 describes the electrical dynamic of the dc motor used.

But substituting equation 5 into 6 we obtained the mechanical equation to be;

$Ki_a - b\dot{\theta} = J\ddot{\theta}$ 10

Taking the Laplace transform of the electrical and mechanical equation in equation 9 & 10,

For electrical: L $(e_a - R_a i_a - L_a \frac{di_a}{dt} - K_b\dot{\theta} = 0)$ 11

$E_a(s) - R_a I_a(s) - L_a S I_a(s) - K_b S\Theta(s) = 0$ 12

For Mechanical: L $(Ki_a - b\dot{\theta}) = L(J\ddot{\theta})$

$KI_a(s) - bS\theta(s) = J\theta$ 13

Eliminating $I_a(s)$, equation 13 is transformed to; $I_a(s) = \frac{(JS^2 + bS)\theta(s)}{K}$ 14

Putting equation 14 into 13 and rearranging, we have

$E_a(s) = [(R_a + SL_a)(JS + b)\frac{S}{K} + K_b S]\,\theta(s)$ 15

By transforming equation 15,

Transfer Function (T.F) $= \frac{\theta(s)}{E_a(s)} = \frac{1}{\frac{S}{K}(R_a + SL_a)(JS+b) + Kbs]}$

To obtain the polynomial, we multiply by $\frac{K}{K}$

$\frac{\theta(s)}{E_a(s)} = \frac{S}{K}(\frac{1}{R_a} + SL_a)(JS + b) + Kbs] \times \frac{K}{K}$

$T.F = \frac{\theta(s)}{E(s)} = \frac{K}{S[(R_a + SL_a)(J_s + b) + KK_b]}$ $(\frac{radian}{V})$ 16

Equation 16 is the transfer function of dynamic model of armature controlled dc motor.

(iii) Photovoltaic Cell (solar panel) Transfer Function

In Figure 2, the photovoltaic characterization include;

(a) The magnitude of the photo current which depends on the following;
i. Irradiance level ii. Light spectrum iii. Characteristics of the cell

(b) Short circuit current which is direct measure of the photon current (I_{Ph}) as specified at Standard Test Condition (STC) are;
* 1000W/m^2 * Module temperature of 25^{0}C * Air mass (AM) = 1.5

(c) Magnitude of photon current (short circuit current) is directly proportional to the irradiance.

(iv) Diode Equation

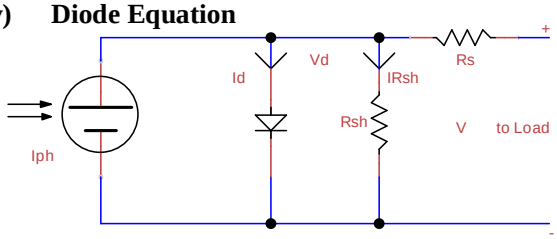

Fig. 2: Photovoltaic cell model

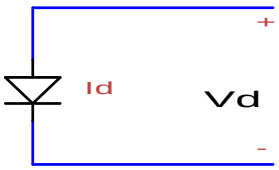

Fig. 3: Diode photovoltaic cell

$$I_d = I_o[e^{\frac{qV_d}{aKT}} - 1] = I_o[e^{\frac{V_d}{V_{TH}}}] \quad 17$$

Where T = Temperature in Kelvin (K), q = Charge of an electron in coulombs (1.602 x 10^{-2} C)
K = Boltzmann constant (1.38 x 10^{-23} JK^{-1})
I_o = Dark or reverse saturation current of the diode at temperature (T).
a = Diode identification factor (normally between 1 & 2)
$V_{TH} = \frac{KT}{q}$ = Thermal voltage (V_{TH}) and is always 25.84mV for silicon at 300K at a = 1
R_{SH} = Shunt resistor (Ω), R_s = Resistor in Series (Ω)
I_{Ph} = Photon current at a given irradiance and at temperature (T), V_d = Voltage across the diode

(a) Series Resistance Equation

From Kirchhoff voltage law, $V_d = V + IR_s$ 18

$$I = I_{ph} - I_o(e^{\frac{q(V+IR_s)}{akT}} - 1) \quad 19$$

(b) Shunt Resistance Equation

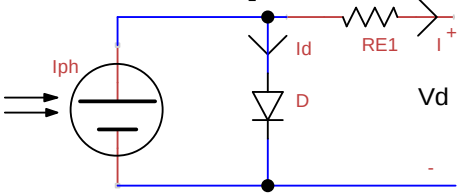

Fig. 4: Series resistance configured photovoltaic cell

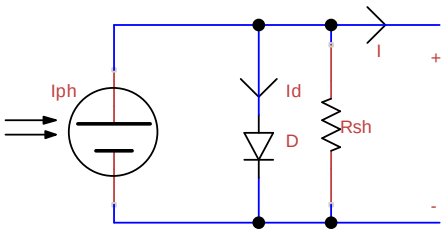

Fig. 5: Shunt resistance configured photovoltaic cell

Recall that;

- R_{sh} models the leakage current of the p-n junction.
- Typical R_{sh} is a large volume, with low values representing defective cells
- Impact (on power loss) more pronounced at low irradiance levels.

For general PV cell equation, we Apply Kirchhoff Voltage (KVL) and current law (KIL) to Figure (5) above, the total current (I) flowing in the circuit becomes;

$$I = I_{ph} - I_d - I_{sh} \quad 20$$

That is; $$I = I_{Ph} - I_o[e^{\frac{V_d}{V_{th}}} - 1] - [\frac{V+IR_s}{R_{sh}}] \quad 21$$

For a maximum possible voltage of PV cell, the circuit is open, I = 0 and V = V_{OC} as shown in Figure 6, where V_{OC} depend on the quality of the material (typically silicon). But considering an ideal PV cell and neglecting resistances as all resistances in the system are less than zero.

From I = I_{Ph} - $I_o[e^{\frac{V_d}{V_{th}}} - 1]$ - $[\frac{V+IR_s}{R_{sh}}]$ 22

(c) Open Circuit Voltage (V_{oc})

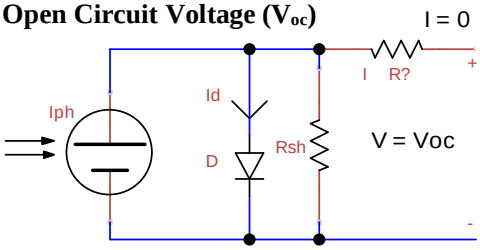

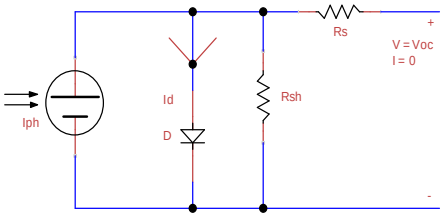

Fig. 6: Complete Photovoltaic Cell Model Fig. 7: Equivalent Photovoltaic cell model showing open circuit voltage

In this case we neglect all resistances and I = 0, therefore equation 22 becomes

$0 = I_{Ph} - I_o[e^{\frac{qV}{akT}} - 1]$

$\frac{I_{Ph}}{I_o} = e^{\frac{qV_{oc}}{akT}} - 1$

Applying In (log) to both sides, $\ln(\frac{I_{Ph}}{I_o} + 1) = \ln(e^{\frac{qV_{oc}}{akT}})$

$V_{oc} = \frac{akT}{q}\ln(\frac{I_{Ph}}{I_o} + 1)$

It can be seen that I_o is a component of temperature, as such V_{oc} is a strong function of temperature dependence with a high negative temperature coefficient.

(d) Short Circuit Current (I_{sc})

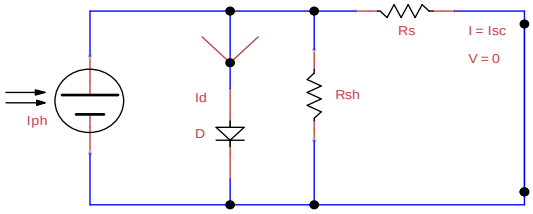

Figure 8: Equivalent photovoltaic Cell Model with Output short

For small values of R_s compared to zero (i.e R_s = 0), the maximum possible current from the PV cell can be calculated as follows;

From (Bana and Saini, 2016), we have that; I = I_{Ph} - $I_o[e^{\frac{V_{oc}}{V_{th}}} - 1]$ - $[\frac{V+IR_s}{R_{sh}}]$

For open circuit; I = I_{sc} and V_{oc} = 0

$I_{sc} = I_{ph}$ 23

The photon generating current is equal to I_{sc} but directly proportional to the irradiance. (Adel, 2010). The change can be calculated using Equation 24.

$I_{ph} = I_{max}\text{Cos}\ \theta$ 24

Two model assumptions based on the solar intensity source are considered;

Assumption 1: Varies and photovoltaic cell is static, Equation 24 holds.

Assumption 2: Varies with respect to the photovoltaic cell, Equation 24 becomes

$I_{sc} = I_{max}\text{Sine}\theta$. But since the goal is to maintain the orthogonality of the solar incident with respect to the solar panel, Equation 23 is substituted into (24), then,

$I_{sc} = I_{max}\text{Sine}\ \theta$ 25

$\frac{I_{sc}}{Sine\ \theta} = I_{max}$

Where; $I_{max} = I_{ph}$ = Maximum photon current (eV), I_{sc} = I = Output current of the PV cell

Therefore, the actual output equation becomes

$I = I_{ph} \text{Sine } \theta$ 26

The transfer function of the PV cell becomes;

$\text{T.F} = \frac{I}{Sine\ \theta} = I_{ph}$ 27

Equation 27 is the transfer function of the photovoltaic cell (solar panel) of the system.

(v) Modeling of the Close Loop Transfer Function of the Cascade Control System

Lets $K_1(s) = T.F_{PI} = \frac{R_2(s)}{E_v(s)} = \frac{K_D S^2 + K_p S + K_I}{S}$ 28

$K_2(s) = T.F_{PI} = \frac{U(s)}{E_\theta(s)} = \frac{K_p S + K_I}{S}$ 29

$M(s) = \text{T.F}_M = \frac{\theta(s)}{E(s)} = \frac{K}{S[(R_a + SL_a)(J_s + b) + KK_b]}$ 30

$P(s) = \text{T.F}_P = I_{ph}$ 31

To evaluate the transfer function of the system, we first consider the transfer function of the inner loop, we use the inspection approach (Anonymous, 2012)

$\text{T.F} = \frac{Forward\ Loop}{1 + Loop\ Transfer\ Function}$ 32

$T.F_{Inner\ Loop}\ \frac{\theta(s)}{r_2(s)} = \frac{K_2(s)M(s)}{1 + K_2(s)M(s)}$ 33

By inspection and using the formula in Equation 32 it becomes,

$$T.F_S = \frac{I(s)}{r_1(s)} = \frac{K_1(s)[\frac{K_2(s)M(s)}{1+K_2(s)M(s)}]P(s)}{1+\frac{K_1(s)K_2(s)M(s)\ \ P(s)}{1+K_2(s)M(s)}}$$

Multiplying $1 + K_2(s)M(s)$ by both the numerator and denominator we arrived at;

$$\boldsymbol{T.F_S = \frac{I(s)}{r_1(s)} = \frac{K_1(s)K_2(s)P(s)}{1+K_2(s)M(s)\ \ + K_1(s)K_2(s)M(s)\ \ P(s)}}$$ 34

But the output Equation becomes;

$I(s) = (\frac{K_1(s)K_2(s)P(s)}{1+K_2(s)M(s)\ \ + K_1(s)K_2(s)M(s)\ \ P(s)})r_1(s)$ 35

Substituting Equations 28, 29, 30 and 31 into 35, it becomes;

$$\frac{I(s)}{r_1(s)} = \frac{\left(\frac{K_D S^2 + K_P S + K_I}{S}\right)\left(\frac{K_P S + K_I}{S}\right)(I_{ph})}{1+\left(\frac{K_P S + K_I}{S}\right)\left(\frac{K}{S[(R_a + SL_a)(J_a + b) + KK_b]}\right) + [(\frac{K_D S^2 + K_P S + K_I}{S})(\frac{K_P S + K_I}{S})(\frac{K}{S[(R_a + SL_a)(JS + KK_b]})(I_{ph})]}$$ 36

Resolving Equation 35 appropriately by simplification, it then becomes;

$$\frac{I(s)}{r_1(s)} = \frac{I_{ph}(K_D K_p S^3 + K_D K_I S^2 + K_p^2 S^2 + 2K_p K_I S + K_I^2)[(R_a + Sla)(Js + b) + KK_b]S}{S^3[(R_a + Sla)(Js + KK_b)] + S(K_p S + K_I)K + I_{ph}(K_D K_p S^3 + K_D K_I S^2 + K_p^2 S^2 + 2K_P K_I S + K_I)}$$ 37

Equation 37 becomes the general close loop transfer function of the cascade control system.

(vi) Open Loop Transfer function of the Main Process Plant

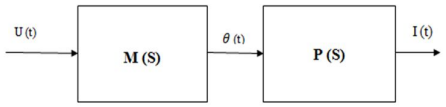

Figure 9: Block Diagram of Open Loop of the Main Process System

The equation of the feedback path of Figure 1a produced;

$I(t) = P(s) \times \theta(t)$ 38

$\theta(t) = M(s) \times U(t)$ 39

Applying Laplace transform to Equation 38 and 39, they become;

$I(s) = P(s) \times \theta(s)$ 40

$\theta(s) = M(s) \times U(s)$ 41

Substituting Equation 41 into 40 produces $I(s) = P(s) \times M(s) \times U(s)$

But by rearrangement we have; $\frac{I(s)}{U(s)} = P(s) \times (M(s)$ 42

Substituting Equation 30 and 31 into 32 we have;

$$\frac{I(s)}{U(s)} = (I_{ph})\left(\frac{K}{S[(R_a+SL_a)(J_s+b)+KK_b]}\right)$$

Therefore, the open loop Transfer Function of the process becomes,

$$\frac{I(s)}{U(s)} = \frac{I_{ph}K}{S[(R_a+SL_a)(J_s+b)+KK_b]} \quad (43)$$

(vii) System Simulink Models and Simulation

All the system mathematical transfer functions are used to construct simulink block for possible simulation as well as obtaining step and frequency response. The step and frequency response is based on the open and closed loop response.

(a) Open Loop Method (Step Response)

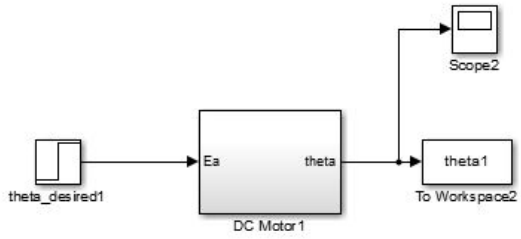

Figure 10: Simulink model of dc motor system

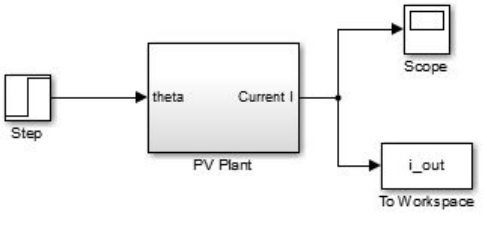

Figure 11: System simulink model of photovoltaic

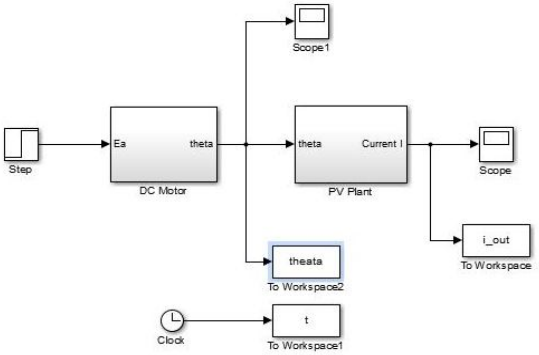

Fig. 12: Simulink diagram of open loop process plant

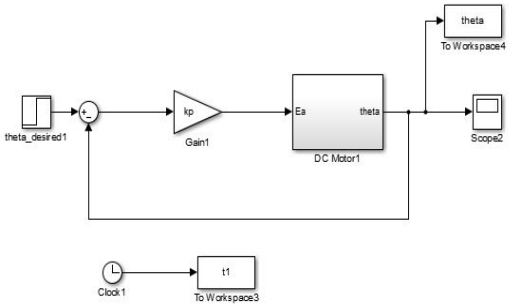

Fig. 13: Simulink model of Kp on dc motor system

(b) Closed loop method (Frequency Response)

Table 1: Zeigler Nichols Tuning Table

Controller type	Kp	Ki	Kd
P	0.5Ku		
PI	0.45Ku	0.54ku/Tu	
PID	0.6KU	1.5Ku/Tu	0.6Ku/Tu

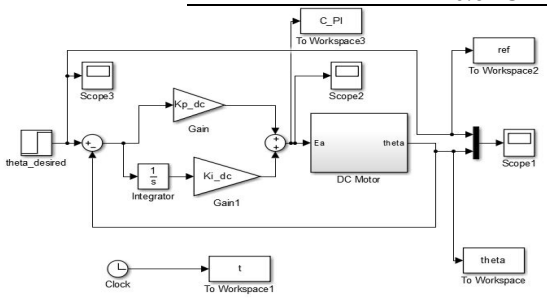

Fig. 14: Closed loop Simulink model of dc motor with controller

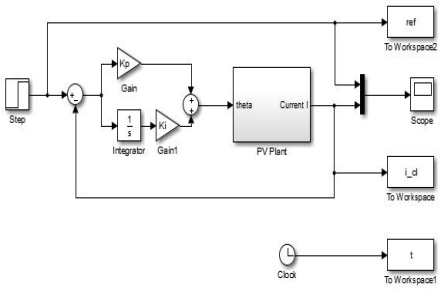

Figure 15: Closed loop Simulink model of PV with PI controller

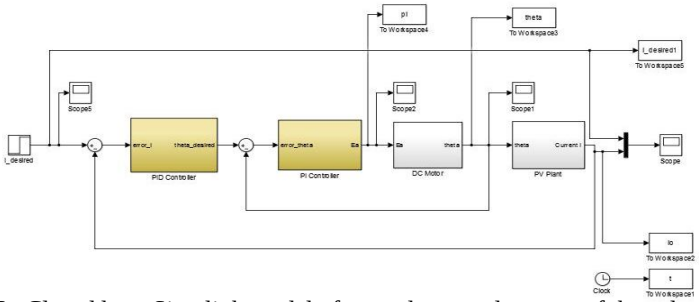

Figure 16: Closed loop Simulink model of cascade control system of the solar tracker

(vii) System Performance

In the existing performance (Ep) with internal model control (IMC-PID) showed that the system rise and settling time are 1.8 sec. and 5.5 sec. respectively (Bamigboye *et al.* 2016). Also, the results summarized in Table 2, shows that our new performance (Np) for rise and settling time are 0.4 sec. and 1.8 sec. respectively. Therefore, to determine our system performance over the existing systems, we have that,

$$\text{Decrease in \% in rise time} = \frac{Existing\ performance\ (Ep) - New\ performance(Np)}{Existing\ performance(Ep)} \text{ x } \frac{100}{1} \qquad 44$$

$$\text{Decrease in \% in rise time} = \frac{1.8-0.4}{1.8} \text{ x } 100 = 77.8\%$$

$$\text{Decrease in \% in settling time} = \frac{5.5-1.8}{5.5} \text{ x } 100 = 67.2\%$$

RESULTS

Figs. 17 to 26 show different signal and frequency response of subsystems and systems models.

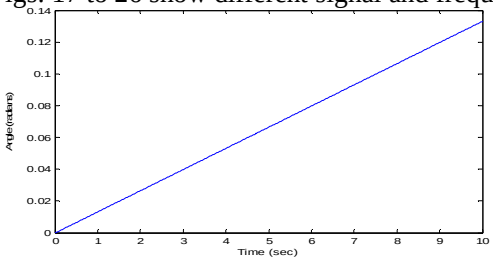

Fig. 17: Open loop step response of dc motor

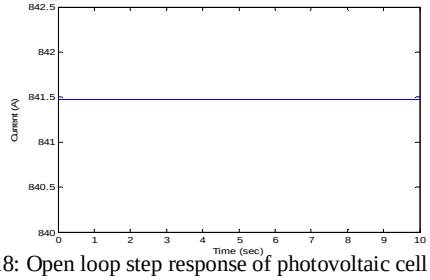

Fig. 18: Open loop step response of photovoltaic cell (PV)

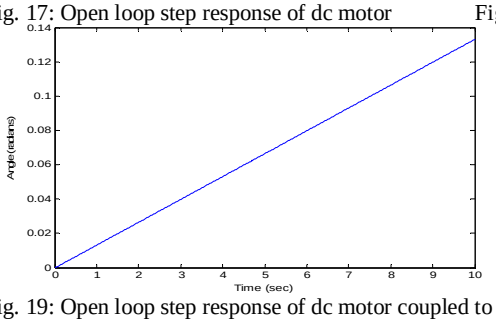

Fig. 19: Open loop step response of dc motor coupled to PV system

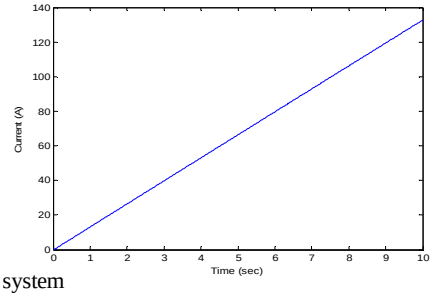

Fig. 20: Open loop step response of the process plant

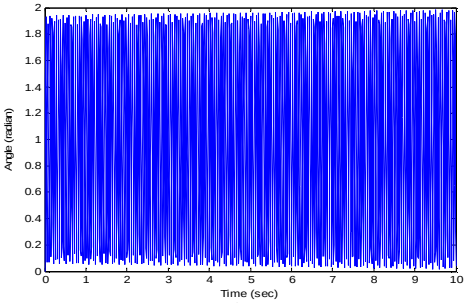

Fig. 21: Frequency response of kp controller on dc motor

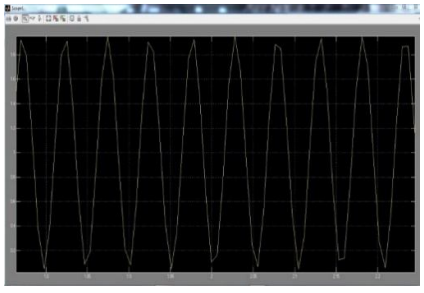

Fig. 22: Freq. response of kp controller on dc motor (zoom)

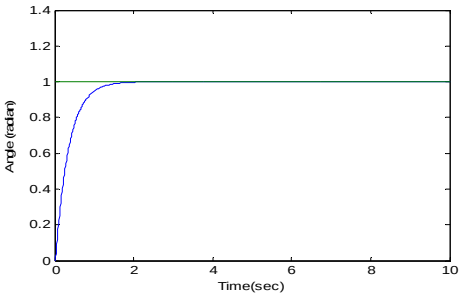

Fig. 23: Output closed loop response of dc motor with controller

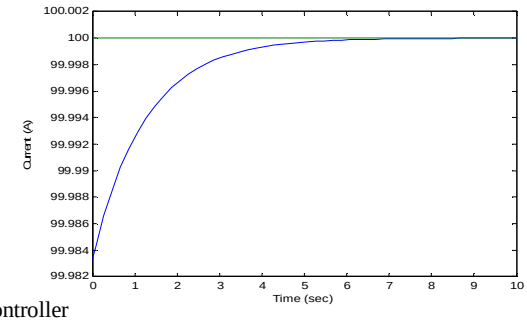

Fig. 24: Closed loop freq. response of PV system with PI controller

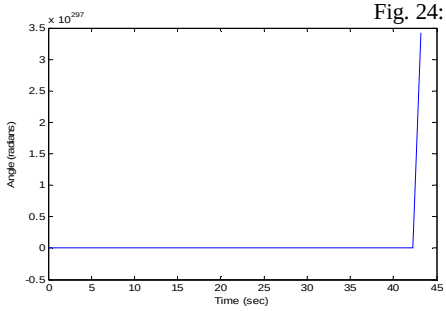

Fig. 25: Time response of dc motor in cascaded system

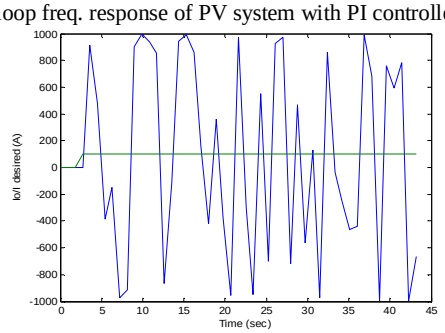

Fig. 26: Frequency response of cascade control system

Table 1: Summary of Open Loop Response (Step Response)

Type of System	Rise Time (sec)	Steady State Error	Settling Time (sec)	Time Delay (sec)
DC motor	Not defined	Not defined	0	0
PV cell	Constant	Not defined	0	0
Cascade	Not defined	Not defined	0	0

Table 2: Summary of Closed Loop Response (Frequency Response)

Type of System	Rise Time (sec)	Steady State Error	Settling Time (sec)	Time Delay (sec)	Overshoot	Undershoot
DC motor	0.4	0	1.8	0	0	0
PV cell	1.6	0	5.5	0	0	0
Cascade	Stable	Stable	Not applied	Not applied	Not applied	Not applied

DISCUSSION

Figure 17 is a step response of an open loop dc motor system. It is obtained from a Simulink block model, when a step input is applied into the input of the dc motor and a corresponding response is obtained across the output of the dc motor. The graph reveals that the dc motor angle is directly proportional to the time. In other words, the output signal continues to increase with increase in time. The system has no overshoot, no offset point, no settling time and no dead time (delay time). It all means that the speed of the dc motor keeps increasing with no sign of steady state. In this case, the dc motor parameters such as speed and torque are not controlled due to the absent of feedback system, and these leads to a continuous increase in speed and torque over time (Yadav, *et al.*, 2014). This means that when a certain step input is applied to the dc motor, the speed and torque of rotation and increases moderately with respect to time.

From table 1, the rise time of open loop dc motor system increases with no settling time, which means that when voltage is applied to the dc motor, the speed and torque becomes unstable as well as the system temperature (Bharathi and Kumar, 2012). Therefore, since the temperature of the system is unstable, it can lead to dc motor damage.

(i) Open Loop Step Response of the Photovoltaic (PV) System

Figure 18 is step response obtained from an open loop Simulink block diagram of photovoltaic system in Figure 11. The response is obtained when a step input signal is applied to the

photovoltaic system and the corresponding output signal called a stem response is obtained. In other words, it is a graph of current plotted against time. The simulated result showed that the current produced by the photovoltaic cell remains constant at 841.5A throughout the time. It also reveals that the output component of the photovoltaic system is independent of time but varies with solar radiation (Dincer and Meral, 2010). The plot shows the difference between the initial and final current, 1.5A. Therefore, this static positioning of the photovoltaic system affects the output component of the photovoltaic cell and it agrees with (Ajao *et al.,* 2013; Shareef, 2017). However, the summary result of an open loop photovoltaic system in Figure 17 has shown that the system has low performance and so it is not considered in the research work.

(ii) Open Loop step response of dc motor in cascaded system

Figure 19 shows a step response of a dc motor in an open loop cascaded system. The output signal is obtained when the dc motor output is coupled to the input of the photovoltaic system (figure 12). An oscilloscope is connected to the output of the dc motor such that the response of the dc motor in the open loop cascade system is obtained. it is also a graph of angle against time. This plot reveals the behavior of dc motor in an open loop cascaded mode. The response of the dc motor cascaded system is similar to Figure 17 when is not in the cascaded. It shows a straight line graph passing through the origin, where the angle is directly proportional to the time. In other words, the dc motor speed and torque increase with time, which means that in an open loop cascade, the dc motor system speed starts rotating from initial, which is from 0^0 to infinite position even with no accuracy. This is so because there is no feedback path which could control both speed and torque and make the system stable and accurate (Rooholahi and Reddy, 2015).

(iii) Closed Loop Frequency response of dc motor for proportional gain (Kp)

Figures 21 to 22 shows the frequency response of a closed loop dc motor system with a proportional gain (Kp). The results are obtained from figure 13, where a proportional controller is used to tune the dc motor to a stable state. In this case, a step input is applied through the summer input and proportional term so as to provide the required voltage to the dc motor input and the corresponding response is obtained at the output. The response obtained at the dc motor output is an undamped oscillation response with equal amplitude. Figure 21 is an amplified response of figure 22, where the amplitude of the response is adjusted so that readings in terms of ultimate gain (Ku) as well as ultimate period (Tu) are taken. The ultimate period (Ku) of the closed loop dc motor using proportional controller is 0.5, while the ultimate gain (Tu) at indefinite steady state oscillation is 20,022. These values agree with other studies that the higher the value of ultimate gain (Tu), the faster, more stable and accurate the system becomes (Kumar, 2013).

(iv) Closed Loop frequency Response of dc motor System

Figure 23 is the frequency response of closed loop dc motor simulated from Fig. 14. It is also a simulated result of angle against time. The plot revealed the action of proportional and integral term effect on the dc motor system with a feedback path. The graph also revealed a closed loop characteristics of dc motor in terms of signal rise time, settling time, overshoot, steady state error which are interpreted into dc motor speed, torque, positioning, accuracy and temperature.

In the simulated result, the signal rises from 0 and the frequency response signal rise time was 0.5 sec., while the settling time was 1.6 sec. (Table 2). It shows that the rise and settling time is relatively moderate as it agrees with other studies (Bamigboge *et al.*, 2016). The plot also shows that there is no overshoot and offset in the system which is a good response from any good proportional and integral controlled system (Rao, 2013). It means that the presence of proportional and integral term acted on the overshoot and offset components, hence propagate and eliminate it completely (table 2). It shows that as the dc motor speed increases rapidly when voltage is applied, the proportional and integral (PI) slave controller (inner loop controller) adjusts in other to reduce the error between the desired and actual speed of the dc motor system which agrees with (Dubey, 2013). Also, it takes 0.5 sec. for dc motor to change its angle or turns and then stabilizes at 1.6 sec. when a certain small voltage is applied. This implies that a small voltage applied to the dc motor will cause it to respond faster and at a moderate speed and torque.

(v) Closed Loop Frequency Response of Photovoltaic Cell (PV) System

Figure 24 is the closed loop frequency response of a photovoltaic cell with proportional and integral (PI) controller. It is a plot of output current against time obtained when the Simulink model in figure 15 was simulated. It revealed the behavior of proportional and integral term action on photovoltaic cell positioning. The frequency response curve shows a relative longer time for the signal to settle at set point (100A) as compared to that of the closed loop frequency response in Figure 23. According to the response curve, it took 1.6 sec. for the signal to rise from its initial point before getting to the settling point, that the rise time. The response also reveals that it took 5.5 sec. for the signal to get settled (settling time). It shows that there is a small delay in the process as it took 1.6 sec. for the signal to rise (Table 2). This implies that the speed is reduced due to the applied load and torque is increased.

(vi) Time response of the dc motor in cascade system.

Figure 29 is the time response of dc motor in the cascade system, the response of angle against time. The signal is obtained when an oscilloscope is connected to the output of the dc motor with respect to time. The output signal revealed the behavior of dc motor in a cascaded control system, especially when it output is coupled to the load (solar panel). The dc motor behavior includes the delay time, speed, rise time and torque. The simulated time response result shows that it took about 40.4 sec. delay time for the dc motor to response to the applied input. The graph also reveals that the dc motor has a moderate speed as the signal rise time increases sharply with a moderate torque. In practice, implies that in the cascade control system, it took some time for the dc motor to start rotating when an input voltage is applied. The time taken for the dc motor to rotate is relatively long but since this is just a simulated result the real time is usually shorter.

(vii) Closed Loop Frequency Response of a cascaded control system (Solar Tracker)

Figure 26 is the closed loop frequency response of a cascaded control system, also known as the closed loop response of the overall system, called solar tracker. It is the output response from the Simulink block diagram of figure 16. That is, the signal is obtained when a step input is applied into the summer junction of the outer proportional controller and the output frequency response is taken from the photovoltaic cell output. The frequency response revealed the overall system behavior especially when all the components are working. The graph shows the rate and possibility of working, including the system stability, accuracy, response time, speed, torque.

CONCLUSION

Modeling, characterization and optimization of solar tracker using proportional integral controller has been achieved. Basic mathematical models have been successfully formulated, built and developed. These mathematical models include transfer function for both inner and outer loop of proportional integral controllers (Master and slave proportional controllers), electrical component of the dc motor, mechanical component of the dc motor, transfer function of the dc motor, input and output component of the photovoltaic cell; that is diode equation, series resistance open circuit voltage equation, short circuit equation and shunt resistance equation. Also, Simulink models of the various sub-systems and the overall cascade control system have been designed and developed using MATLAB software. The sub-systems include; proportional controller transfer function, electrical and mechanical components of the dc motor transfer function, photovoltaic cell transfer function and the overall system transfer function. Also, simulation of subsystems models has been carried out with different time and frequency responses fantastically obtained. The results obtained shows that the subsystem and system models have worked as anticipated. The experimental simulation results of various subsystems of proportional integral controller with dc motor, proportional integral controller with photovoltaic cell and overall cascade control system time responses which showed a reduced percentage system rise time by 77.8%, settling time by 67.2%. The responses also showed no overshoot but eliminated steady state error. It is seen that the use of proportional controllers in solar tracking system has improved the tracking stability characteristics in terms of desired speed, positioning, tolerance, time and frequency response. However, it is recommended that further

research should also be carried out on the methods of cooling and maintaining photovoltaic cell temperature as well as advance controllers, as it will boast solar panel efficiency.

REFERENCES

Adel, E. S. (2010). PV Cell Module Modeling & ANN Simulation for Smart Grid Applications. *Journal of Theoretical and Applied Information Tech.*

Ajao, K. R., Ambali, R. M. and Mahmoud, M. O. (2013). Determination of the Optimal Tilt Angle for Solar Photovoltaic Panel in Ilorin, Nigeria. *Journal of Engineering Science and Technology Review*, 6(1): 87-90.

Anonymous (2012). Transfer Function Models of Dynamical Processes. www.chemeng.queensu.ca/courses/CHEE319/documents/CHEE319_notes_2012_lecture4.pdf. Retrieved on 3rd September 2018.

Balabel, A., Mahfouz, A. A. and Salem, F. A. (2013). Design and Performance of Solar Tracking Photo-Voltaic System; Research and Education. *International journal of control, automation and system*, 1(2): 49–55.

Bamigboye O., Oladayo and Adewunmi O. T. (2016). Development of Solar Tracking System Using Imc-Pid Controller. *American Journal of Engineering Research*, 5(5): (1-8).

Bana, S. and Saini, (2016). A mathematical modeling framework to evaluate the performance of single diode and double diode based SPV systems. *ScienceDirect*. 2, 171-187.

Baranwal, A. and A. Dwived, A (2014). Optimization of solar energy using solar tracking system. *National Conference on Futuristics in Mechanical Engineering. Available at: www.researchgate.net/profile/abhishek_dwivedi12*. Retrieved on 12th January 2018

Bharathi, M. and Kumar, G. (2012). Design approach for pitch axis stabilization of 3-dof helicopter system and lqr controller. *International Journal of Advanced Research in Electrical, Electronics and Instrumentation Engineering*, 1(5): 351-365.

Dincer, F. and Meral, M. E. (2010). Contrical factor that affecting efficiency of solar cells. *Smart Grid and Renewable Energy Scientific Research* 1: (47 - 50).

Dubey, S. and Srivastava, S. K. (2013). A PID controlled real time analysis of dc motor. *International Journal of Innovative Research in Computer and Communication Engineering*, 1(8): 1965-1973.

Kalanithi, B. and Rajesh, S. (2014). MPPT Controller based solar tracking system. *Journal of Mechanical and Civil Engineering*, 78–83.

Kiyak, E. and Gol, G. (2016). A comparison of fuzzy logic and PID controller for a single-axis solar tracking system. *Springer Open journal*, 1 – 14.

Kumar, N. and Sharma, N. (2016). Improve performance of PV system by PID controller. *International Journal of Science, Engineering and Technology*, 4(1): 227 – 232.

Kumar, R., Sunil, K. Singla, S. K. and Vikram (2013). A Comparative Analysis of different Methods for the tuning of PID Controller. *International Journal of Electronics Communications and Electrical Engineering*, 3(2): 1 – 17.

Ozerdem, O. C. and Shahin, A. (2014). A PV solar tracking system controlled by Arduino/Matlab/Simulink. *International Journal on Technical and Physical Problems of Engineering*, 6(4): 5-10.

Rao, V. M. V. (2013). Performance Analysis of speed Control of Dc motor Using P, PI, and PID controllers. *International Journal of Engineering Research & Technology*, 2(5): 60 – 67.

Rooholahi, B. and Reddy, P. L. (2015). Concept and application of PID control and implementation of continuous PID controller in Siemens PLCs. *Indian Journals of science and Technology*, 8(35): 1 – 9.

Shareef, S. J. (2017). The impact of tilt angle on photovoltaic panel output. *ZANCO Journal of Pure and Applied Science*, 29 (5): 112 – 118.

Sparavigna**,** A. C. (2015). A historical discussion of angular momentum and its Euler equation. *International Journal of Sciences***.** 1(07): 34 - 38.

Yadav, M., Kanodia, K, and Kumari, N. (2014). Review paper on controlling the speed of Dc motor with high accuracy and demerits of other speed controlling techniques. *International Journal of Enhanced Research in Science Technology & Engineering*, 3(11): 73 – 77.